JJEE
Volume 3, Number 4, 2017
Pages 208-222
Jordan Journal of Electrical Engineering
ISSN (Print): 2409-9600, ISSN (Online): 2409-9619

# Turn-to-Turn Short Circuit Faults between Two Phases in Permanent Magnet Synchronous Motor Drives

Mounir Hadef[1], Mohamed R. Mekideche[1], Abdesslem Djerdir[2], Abdoul O. N'diaye[2]

[1]L2EI Laboratory, University of Jijel, Jijel, Algeria
[2]IRTES-SET Laboratory, University of Technology of Belfort-Montbeliard, Belfort Cedex, France
e-mail: hadef_mounir@yahoo.fr

*Received: October26, 2017* *Accepted:November18, 2017*

***Abstract***—With the increased use of permanent magnet synchronous motors (PMSMs), efficient online condition monitoring and accurate fault diagnosis for these machines are very important. In order to reduce downtime and avoid unsafe operating conditions, it is essential to establish a methodology capable to detect incipient turn faults. This paper analyzed the consequences of turn-to-turn circuit faults between two phases in a PM synchronous motor. Thus, a simple method based on rotor speed ripples is proposed for detecting stator winding faults. Also, a fault index allows quantifying the severity of the fault. This latter seems to be well adapted for PM motors health monitoring and interturn fault diagnosis. Experimental results are included to show the ability of the proposed strategy to detect incipient faults.

***Keywords***—Interior permanent magnet synchronous motor, Fault detection and diagnosis (FDD), Space vector pulse width modulation (SVPWM), Stator winding faults modeling, Vector control.

## I. INTRODUCTION

Permanent magnet synchronous motors have been widely used in electric drive applications for their high efficiency and power density over other kinds of traditional motors like dc motors or induction motors. However, PM motors are under a great variety of abnormal operations including faults [1]-[4]. These faults create special challenges for a PMSM due to the presence of the spinning rotor magnet that cannot be stopped during faults. Stator windings short circuit is one of the most common fault in electrical machines. Interturn short circuits usually result from insulation faults caused by system transients, overloading, environmental related issues or manufacturing design defects [1], [5]-[8].

Fault detection and diagnosis (FDD) of electrical machines have been systematically pursued by many works during the last decades; and have become a major topic of concern among industrial and academic research [1]-[2], [5], [7], [9], [10]-[12]. Unexpected failures in electrical motors may indeed lead to important losses in production and additional costs. For these reasons, developing efficient and robust diagnosis systems is a priority for electrical machines manufacture. Traditional FDD methods can be classified into three categories: quantitative model based methods, qualitative model based methods, and process history based methods. Furthermore, there have been several published methods regarding mechanical or electrical faults mitigation in electrical machines [5], [9], [13]-[19].

In [1], a novel scheme for PMSMs health monitoring and fault diagnosis has been proposed. The faults in this study include static and dynamic eccentricity, interturn short circuit, phase-to-ground short circuit, and partial and uniform demagnetization. In [2], the authors proposed an alternative technique using an inverter embedded for automated detection and classification of demagnetization and eccentricity for PMSMs. According to the results, the proposed technique has such advantages as high sensitivity, high reliability and low cost. A fault model of an inverter-fed PM synchronous motor is derived using the line voltage, which

Corresponding author's e-mail: hadef_mounir@yahoo.fr

can be effectively used to evaluate the performance of a fault detection algorithm [3]. In [4], this paper studies interturn short circuit fault detection in PMSMs using an open-loop physics-based back electromotive force estimator. Fault detection system leads to discriminative interturn fault signatures in a fraction of a second for a wide speed range. A study of the effects of different stator winding configurations in both of the stator currents and the zero-sequence voltage component (ZSVC) spectra of healthy and faulty PMSMs has been proposed [5]. In [6], the authors develop an interturn short fault model of PMSM, employing series and parallel winding connections based on deformed flux modeling of the linkage between the same phase windings. Uresty and others [7] proposed two detection methods: the third harmonic of the stator currents and the first one of the zero-sequence voltage component. Two reliable fault indicators for detecting stator winding interturn faults under nonstationary speed conditions are presented. In [8], the authors developed an interturn short circuit fault model for PMSMs, using a deformed flux model with respect to the variations in inductance and back EMF term. In [9], by analyzing the stator current, a Hilbert-Huang transformation is applied to detect the very early stage fault in interturn insulation in permanent magnet synchronous wind generators (PMSWG). In [15], an analytical model of the PM motors when operating under stator faults is developed. Saleh et al. [16] proposed implementing an embedded digital protection for a PMSM drives, which are established through extracting the high-frequency sub-band present in the *d-q* components of the currents. In [17], a review of existing techniques available for online stator interturn fault detection and diagnosis in electrical machines is presented. Two short circuit fault models of a hybrid excitation flux switching PM motor are presented. Based on this model, two cases of short circuits have been studied. The first is the excitation phase short circuit; and the second is the interturn short circuit in excitation winding [20]. Aubert and others [21] proposed a fault indicator for interturn short circuit detection in PMSGs, which allows localizing the faulty phase and is sensitive to resistive interturn short circuits. In [22], the authors proposed an analytical model to evaluate the interturn short circuit fault of a PMSM by computing self and mutual inductances. The model was verified with finite element method (FEM). In [23], the paper introduces an enhanced least-squares (LS) estimation algorithm that incorporates a function for correcting the estimation bias, which is a forgetting factor for capturing sudden faults, and a recursive structure for efficient real-time implementation on a PM stator windings. In [24], the authors proposed a simple and effective torque-ripple minimization method for the torque predictive control (TPC) of PMSMs.

This paper is organized as follows: section II gives modeling details of a three-phase PMSM suffering from two phases winding turn faults. Section III describes the space vector pulse width modulation (SVPWM) technique. The principle of field-oriented control (FOC) of a PMSM is presented in section IV. The results of experimental tests of two phases winding faults are presented in section V. Finally, section VI gives concluding remarks.

## II. MODELLING OF TWO-PHASES WINDING TURN FAULTS

A short-circuit in the stator effectively introduces extra winding in the motor's winding structure. A three-phase star-connected stator winding with two short-circuits on the stator phase *a* and *b* is shown in Fig. 1. The phases *a* and *b* windings are described with two subwindings $a_1$, $a_2$ and $b_1$, $b_2$ in series respectively. Subwindings $a_2$ and $b_2$ are shorted via the resistors $R_{af}$ and $R_{bf}$ to model the short circuit fault.

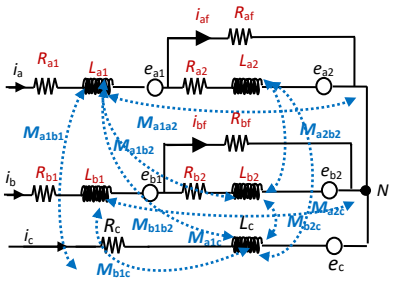


Fig. 1. Equivalent circuit of PMSM with an interturn fault in phase *a* and *b*

The voltage equation is written as follows:

$$[v_s]=[R_s][i_s]+[L_s]\frac{d}{dt}[i_s]+[e_s] \tag{1}$$

where

$$[v_s]=[v_a \;\; v_b \;\; v_c \;\; 0 \;\; 0]^T,\quad [i_s]=[i_a \;\; i_b \;\; i_c \;\; i_{af} \;\; i_{bf}]^T,\quad [e_s]=[e_a \;\; e_b \;\; e_c \;\; e_{a2} \;\; e_{b2}]^T$$

The inductance and resistance matrices are given as in (2) and (3):

$$[L_s]=\begin{bmatrix} L_a & M & M & -(L_{a2}+M_{a1a2}) & -(M_{a1b1}+M_{a2b2}) \\ M & L_b & M & -(M_{b1a1}+M_{b2a2}) & -(M_{b1b2}+L_{b2}) \\ M & M & L_c & -M_{ca2} & -M_{cb2} \\ L_{a2}+M_{a2a1} & M_{a2b1}+M_{a2b2} & M_{a2c} & -L_{a2} & -M_{a2b2} \\ M_{b2a2}+M_{b2a1} & L_{b2}+M_{b2b1} & M_{b2c} & -M_{b2a2} & -L_{b2} \end{bmatrix} \tag{2}$$

$$[R_s]=\begin{bmatrix} R_a & 0 & 0 & -(R_{a2}+R_{af}) & 0 \\ 0 & R_b & 0 & 0 & -(R_{b2}+R_{bf}) \\ 0 & 0 & R_c & 0 & 0 \\ R_{a2} & 0 & 0 & -(R_{b2}+R_{bf}) & 0 \\ 0 & R_{b2} & 0 & 0 & -(R_{b2}+R_{bf}) \end{bmatrix} \tag{3}$$

where $R_{a,b,c}$ are the stator phase resistances; $R_{a2}$ and $R_{af}$ are the resistance of subwinding $a_2$ and the contact resistance due to the turn-to-turn short, respectively. $R_{b2}$ and $R_{bf}$ are the resistance of subwinding $b_2$ and the contact resistance due to the turn-to-turn short, respectively. $L_{a,b,c}$ are the phase stator inductances. $L_{a2}$ denotes the stator inductance of the faulty subwinding $a_2$. $L_{b2}$ denotes the stator inductance of the faulty subwinding $b_2$. $M_{a1a2}$, $M_{a2b1}$, $M_{a2b2}$ and $M_{a2c}$ are mutual inductances between $a_2$ and $a_1$, $b_1$, $b_2$ and $c$. $v_a$, $v_b$, and $v_c$ are stator voltages of phase $a$, $b$ and $c$, respectively. $i_a$, $i_b$, $i_c$ are stator currents of healthy phases $a$, $b$ and $c$, respectively. $i_{af}$ and $i_{bf}$ are stator currents of faulty phases $a$ and $b$. $e_a$, $e_b$, and $e_c$ are back-EMF of healthy phases $a$, $b$ and $c$, respectively. $e_{a2}$ and $e_{b2}$ are the back-EMF of the faulty phases $a$ and $b$.
The faulty resistances $R_{a2}$ and $R_{b2}$ of subwindings $a_2$ and $b_2$ are respectively given as:

$$\begin{cases} R_{a2}=\mu_a R_a \\ R_{b2}=\mu_b R_b \end{cases} \tag{4}$$

The faulty inductance $L_{a2}$ of subwinding $a_2$ and mutual inductances between healthy subwindings $a_1$, $b_1$, winding $c$, faulty subwinding $b_2$ and faulty subwinding $a_2$ are given as:

$$\begin{cases} L_{a2} = \mu_a{}^2 L_a \\ M_{a2a1} = \mu_a(1-\mu_a)L_a \\ M_{a2b1} = \mu_a(1-\mu_b)M \\ M_{a2c} = \mu_a M \\ M_{a2b2} = \mu_a\mu_b M \end{cases} \quad (5)$$

The faulty inductance $L_{b2}$ of subwinding $b_2$ and mutual inductances between healthy subwindings $a_{1,}$ $b_1$, winding $c$, faulty subwinding $a_2$ and faulty subwinding $b_2$ are given as:

$$\begin{cases} L_{b2} = \mu_b{}^2 L_b \\ M_{b2b1} = \mu_b(1-\mu_b)L_b \\ M_{b2b1} = \mu_b(1-\mu_a)M \\ M_{b2c} = \mu_b M \\ M_{b1a1} = (1-\mu_b)(1-\mu_a)M \end{cases} \quad (6)$$

Where $\mu_a$ and $\mu_b$ denote the fractions of shorted turns of subwindings $a_1$ and $b_2$. $M$ is the mutual inductance between phase windings of healthy PMSM.
The electromagnetic torque can be expressed in *abc*-variables as:

$$T = \frac{e_a i_a + e_b i_b + e_c i_c - e_{a2} i_{af} - e_{b2} i_{bf}}{\Omega} \quad (7)$$

where $\Omega$ is the mechanical angular speed.
The mechanical equation is given as follows:

$$J\frac{d\Omega}{dt} = T - T_L - f\Omega \quad (8)$$

where $T_L$ is the load torque; $J$ and $f$ are moments of inertia and viscous friction coefficient, respectively.

## III. SPACE VECTOR PULSE WIDTH MODULATION (SVPWM)

The SVPWM is a more sophisticated technique for generating a fundamental sine wave that provides a higher voltage to PMSM [25], [26]. It refers to a special way to determine a switching sequence of three-phase voltage inverters; and it uses basic space vectors to generate output voltages to the motor. With a three-phase voltage source inverter (VSI) (Fig. 2), there are eight possible switching states. The two states, from which no power gets transferred from source to load, are termed as null vectors or zeros states noted by $V_0$(000) and $V_7$ (111). The other six states called active states are denoted by $V_1$(100), $V_2$(110), $V_3$(010), $V_4$(011), $V_5$(001) and $V_6$(101).
As shown in Fig. 2, the active states can be represented by space vectors. They divide the space vector plane into six equal sectors. The angle between any two adjacent non-zero vectors is 60 degrees. The two zero vectors are at the original point. The reference voltage $V_r$ can be expressed as a combination of two adjacent vectors. For example, $V_r$ in sector I is expressed as:

$$V_r = \frac{T_1}{T_s}V_1 + \frac{T_2}{T_s}V_2 \tag{9}$$

$V_1$ and $V_2$ are two adjacent voltage space vectors; and $T_1$ and $T_2$ refer to switching on time periods of these voltage vectors. $T_s$ is the sampling period.
The on-durations of the switching state vectors $V_1$ and $V_2$, can be calculated as:

$$\begin{cases} T_1 = \sqrt{3}T_s \dfrac{|V_r|}{V_{dc}} \sin\theta_r \\ T_2 = \sqrt{3}T_s \dfrac{|V_r|}{V_{dc}} \sin(\dfrac{\pi}{3} - \theta_r) \end{cases} \tag{10}$$

where $V_{dc}$ is DC-link; $\theta_r$ is the angle of $V_r$.
The on-duration of zero vector$T_0$ can be calculated as:

$$T_0 = T_s - T_1 - T_2 \tag{11}$$

From Fig. 3, it is obvious that the sector number is determined by the angle of the reference vector.

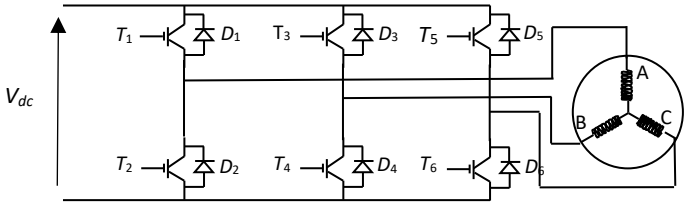


Fig. 2. Three phase voltage type inverter

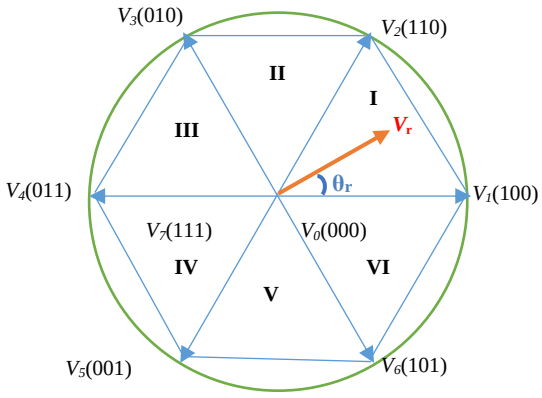


Fig. 3. Voltage vector diagram of SVPWM-VSI

To generate the SVPWM waveforms, the three-phase operation times of PWM are determined in sector III:

$$\begin{cases} T_a = \dfrac{1}{4}\left[T_s - (T_1 + T_2)\right] \\ T_b = T_a + \dfrac{T_1}{2} \\ T_c = T_a + T_1 + \dfrac{T_2}{2} \end{cases} \quad (12)$$

In all of the six sectors, the three-phase operation time is given in Table 1.

TABLE 1
SECTOR NUMBER VERSUS THREE-PHASE OPERATION TIMES

| N | I | II | III | IV | V | VI |
|---|---|---|---|---|---|---|
| Tcom1 | $T_b$ | $T_a$ | $T_a$ | $T_c$ | $T_c$ | $T_b$ |
| Tcom2 | $T_a$ | $T_c$ | $T_b$ | $T_b$ | $T_a$ | $T_c$ |
| Tcom3 | $T_c$ | $T_b$ | $T_c$ | $T_a$ | $T_b$ | $T_a$ |

By comparing the three-phase operation times with the triangular carrier waveform, SVPWM waveforms are generated. With SVPWM control signals, the inverter is switched on or off; and the desired voltage output is produced.

## IV. FIELD ORIENTED CONTROL (FOC) OF PMSM

The goal of the FOC is to perform real-time control of torque variations demand, control the rotor mechanical speed and regulate phase currents in order to avoid current spikes during transient phases [27]. Fig.4 shows the block diagram of the field-oriented control system. The electromagnetic torque $T_e$ can be controlled by the regulation of currents $i_d$ and $i_q$ in a closed loop.

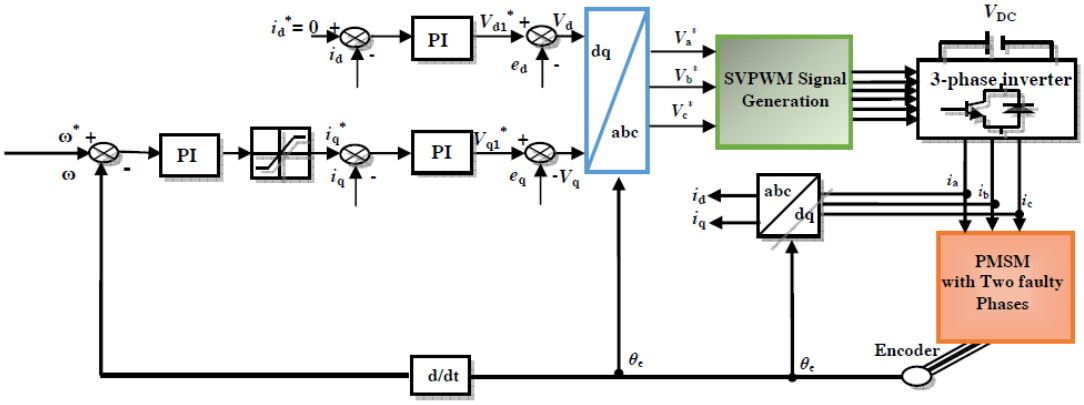


Fig. 4. Block diagram of the proposed control system

The direct current $i_d$ corresponds to the component of a stator magnetic field along the axis of the rotor magnetic field, while the quadrature-axis current $i_q$ corresponds to the orthogonal component. The direct component of the stator current $i_d$ is used as a control quantity for the rotor flux. Maintaining a constant rotor flux obtains a motor torque that is proportional to the quadrature component $i_q$.

The direct reference current $i_d^*$ is set to zero, so as to nullify the reluctance torque of the PMSM. An outer speed loop controlling the inner current loop exists on the quadrature axis. In this inner loop, the actual $i_d$ and $i_q$ currents are compared with their references to find the desired voltages $V_d^*$ and $V_q^*$, which are then transformed into three-phase desired voltage

values $V_a^*$, $V_b^*$, and $V_c^*$ by Park transformation. Once the desired three-phase voltages are obtained, the gating signal generator computes the gating signals for a three-phase voltage source inverter (VSI). The PMSM is fed by the VSI using SVPWM technique.

## V. EXPERIMENTAL RESULTS

A complete drive system has been built; and an experimental study has been carried out to verify the theoretical analysis. The experimental setup consists of a three-phase IPM synchronous motor with three pairs of poles, 1kW, supplied by a dc bus via a voltage source inverter. Table 2 summarizes the specifications of the proposed motor as shown in Fig. 5. The IPMSM under test was loaded by a mechanical torque. Currents of the motor have been sampled by a data acquisition system. The rotor position and speed are measured by an encoder having a resolution of 1024 pulses per mechanical turn. The motor is controlled using the dSPACE DS 1103 real-time platform. The stator windings were modified by the addition of six connections to the stator coils for two-phases *a* and *b* as shown in Fig. 6.

This configuration allows the analysis of short circuit faults among at least 5% and at most 27% of short circuited turns of phase *a* and respectively 7% and 25% of phase *b*. Nine experimental tests were performed on the healthy and shorted stator motor by varying the level of the short circuited turns between phase *a* and phase *b*.

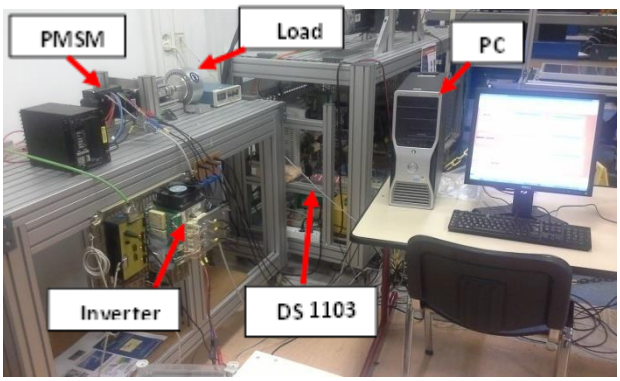


Fig. 5. Experimental setup

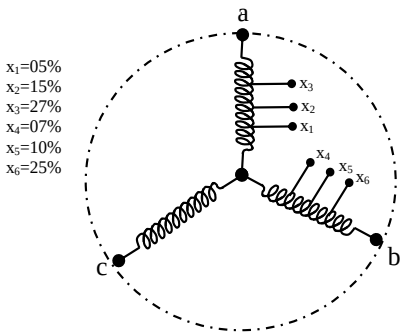


Fig. 6. Stator winding configuration of the PMSM under test

TABLE 2
SPECIFICATION OF THE PROPOSED THREE PHASE PMSM

| | |
|---|---|
| Rated torque ($T_n$) | 3.2 N.m |
| Rated current ($I_n$) | 9 A |
| FEM induced phase ($K_e$) | 33 V/1000 tr/min |
| Maximum current ($I_{max}$) | 33 A |
| Rated speed ($N_n$) | 3000 tr/min |
| Maximum speed ($N_{max}$) | 6000 tr/min |
| Inertia ($J$) | 1.8 Kg.cm$^2$ |
| Stator resistance per phase ($R$) | 0.8 Ω |
| Stator Inductance per phase ($L$) | 3.2 mH |
| Weight ($M$) | 5.6 Kg |

### *A. PMSM Performances in both Healthy and Faulty Conditions*

The specifications of experiments are shown in Table 3, where SCT means the short circuited turns; $t_{sh}$ is the time of short circuit occurring; $\omega_i$ is the initial speed in healthy case; and $\omega_f$ is the speed at the final acquisition time $t$=2.5s.

From Fig. 7a, we can observe that when a fault occurs on two of the three phases, an important arising of the current appears particularly in the corresponding phases. For example, the peak value of the $i_\beta$ current equals 1.88A in healthy conditions. However, this value increases to 3.305A in faulty conditions. Furthermore, we can notice an unbalanced change in the current waveforms, and a continued operation of the faulty phases.

Fig. 7b shows the αβ currents waveforms of the two faulty phases with 7% of short circuited turns of phase *b* and 15% of short circuited turns of phase *a*. The state fault is expressed by an unbalance of the αβ currents. As mentioned previously, an interturn short circuit principally affects the stator current of the faulty phases in a peak value as shown in Fig. 7b, where the peak value of $i_\beta$ current increases from 1.88A in healthy conditions to 4.14A in faulty conditions. Thus, despite the two short circuit faulty phases, the motor continues to operate.

The evolution of αβ components of the stator currents under normal and faulty conditions (7% of short circuited turns of phase *b* and 27% of short circuited turns of phase *a*) is shown in Fig. 7c. The unbalance is apparent; and changes in peak of the two currents are noticeable. Here, the peak value of $i_\beta$ current in faulty conditions is 3.21 times larger than the healthy conditions case (1.88A). Based on the figure at $t$=2.25s, we remark a strong increase of $i_\beta$ current with no continued operation of the faulty phases. The rotor speed for the three fault tests (x14, x24 and x34) is displayed in Fig. 8. As shown in Table 3, the speed decreases with 187 rpm in the cases of x14, 210 rpm and x24, and 330 rpm in the case of x34, after the fault is introduced at t=0.8s, t=1.4s and t=1.52s, respectively. Extra harmonics caused by the fault are clearly observed in the speed curves. These phenomena actually represent typical symptoms for the PMSM operating under such asymmetrical state faults. Fig. 9a and Fig. 9b show the evolution of the αβ components of the stator currents, where 10% of turns of phase *b* are short circuited with 5% and 15% of turns of phase *a*, respectively.

TABLE 3
SPECIFICATION OF EXPERIMENT TESTS

| **Test** | **Type** | **SCT(a), %** | **SCT(b), %** | | **$t_{sh}$, s** | **$\omega_i$, rpm** | **$\omega_f$, rpm** |
|---|---|---|---|---|---|---|---|
| 1 | x14 | 5 | 7 | | 0.80 | 690 | 503 |
| 2 | x24 | 15 | 7 | | 1.40 | 690 | 480 |
| 3 | x34 | 27 | 7 | | 1.52 | 690 | 360 |
| 4 | x15 | 5 | 10 | | 1.40 | 690 | 500 |
| 5 | x25 | 15 | 10 | | 1.49 | 690 | 480 |
| 6 | x35 | 27 | 10 | | 1.35 | 690 | 210 |
| 7 | x16 | 5 | 25 | | 1.35 | 690 | 200 |
| 8 | x26 | 15 | 25 | | 0.98 | 690 | 170 |
| 9 | x36 | 27 | 25 | | 1.35 | 680 | 208 |

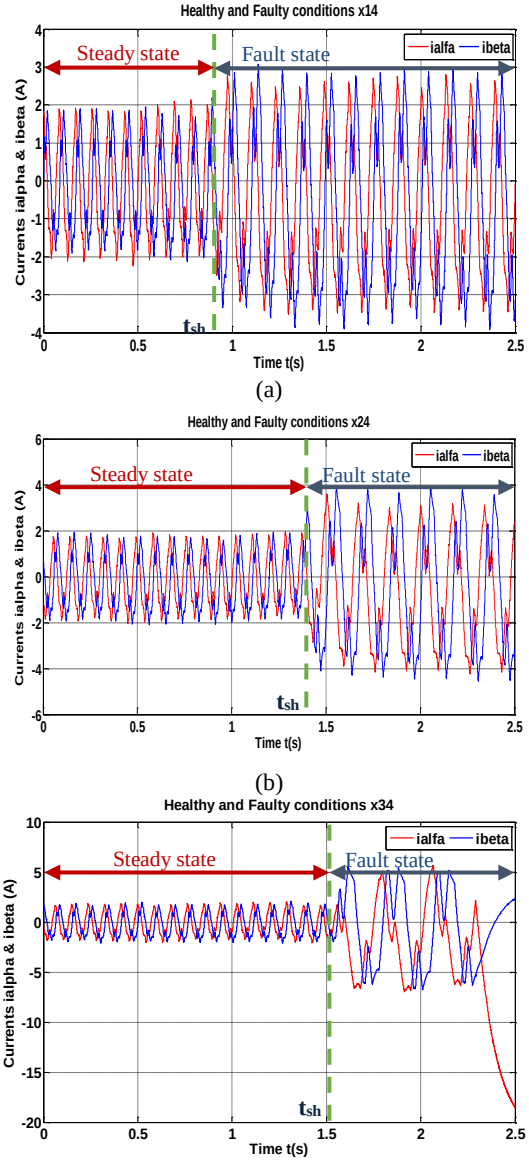


Fig. 7. Experimental current waveforms: a) 5% of SCT phase *a* and 7% of SCT phase *b*, b) 15% of SCT phase *a* and 7% of SCT phase *b*, c) 27% of SCT phase *a* and 7% of SCT phase *b*

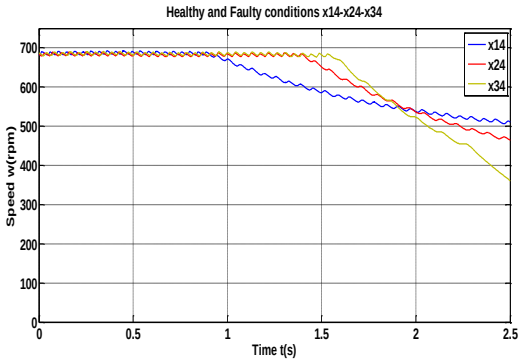


Fig. 8. Speed before and after phase-to-phase short circuit

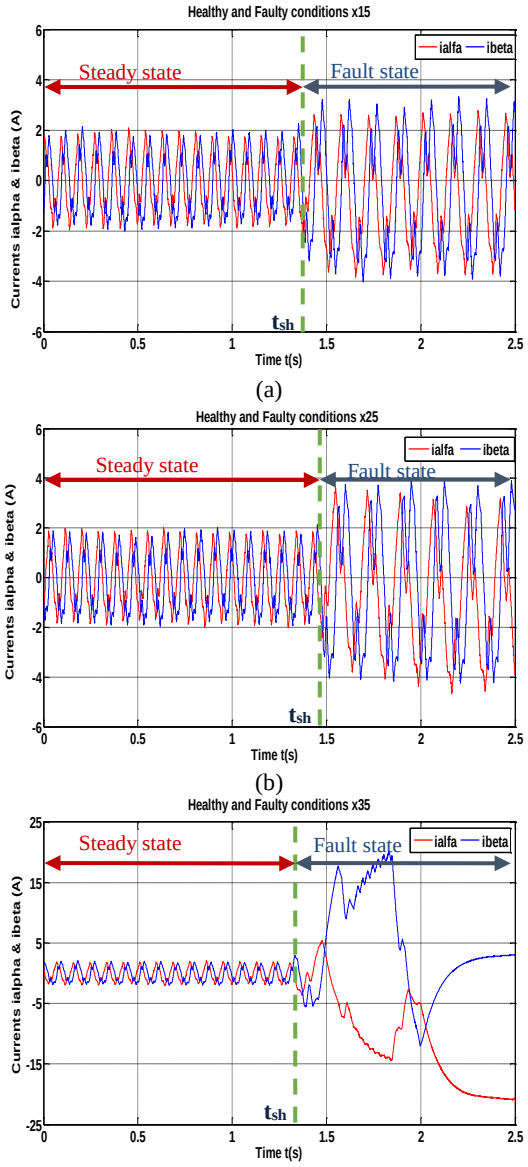


Fig. 9. Experimental current waveforms: a) 5% of SCT phase *a* and 10% of SCT phase *b*, b) 15% of SCT phase *a* and 10% of SCT phase *b*, c) 27% of SCT phase *a* and 10% of SCT phase *b*

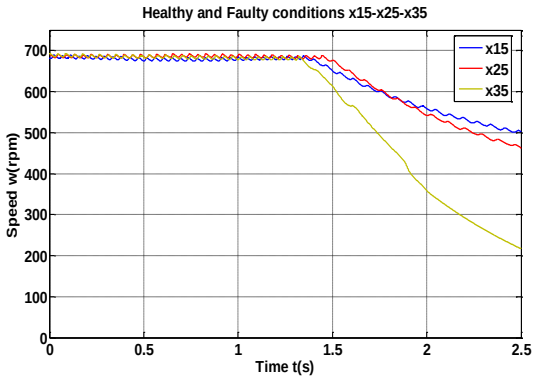


Fig. 10. Speed before and after phase-to-phase short circuit

After the fault occurrence, the peak value of $i_\beta$ current increases from 1.88A to 3.431 A in the case of Fig. 9a and 3.812A in the case of Fig. 9b. The currents from both figures (Fig. 9a and b) have unbalanced changes in the current rms values. In the event of short circuit winding

fault between two phases, where 10% of turns of phase *b* are short circuited with 27% of turns of phase *a*, one can observe a significant peak value of $i_{\alpha\beta}$ currents. The motor cannot continue to operate in these conditions (Fig. 9c). Furthermore, Fig. 10 shows the rotor speed variation in the three fault tests (x15, x25 and x35). Comparing this measured profile based on Table 3, we find that the rotor speed decreases with 190 rpm in the case of x15 test, 210 rpm in the case of x25 test and finally 480 rpm in the case of x35 test. The PM motor cannot follow the control.

In Fig. 11, where 25% of turns of phase *b* are short circuited with 5% , 15% and 27% of turns of phase *a* respectively, it can be observed that when the fault occurs the αβ components of the stator currents become more and more unbalanced and not sinusoidal and then the motor cannot continue to operate. As a result of the fault, the ripple on the speed increases while the overall torque produced by the machine decreases. Similarly, as shown in Fig. 12, the rotor speed decreases with 490 rpm in the case of x16 test, 520 rpm in the case of x26, and finally 472 in the case of x36.

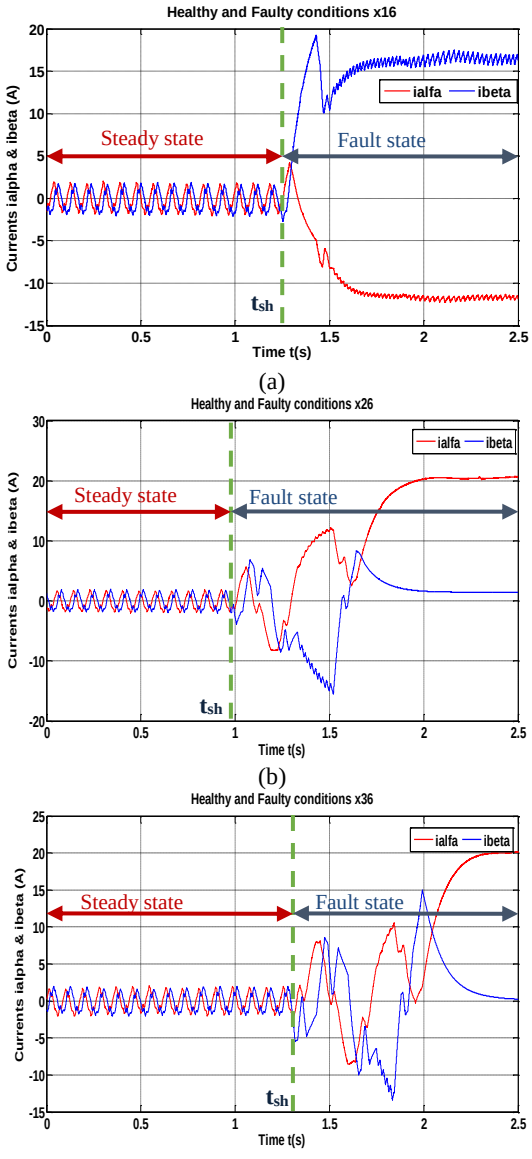


Fig. 11. Experimental current waveforms: a) 5% of SCT phase *a* and 25% of SCT phase *b*, b) 15% of SCT phase *a* and 25% of SCT phase *b*, c) 27% of SCT phase *a* and 25% of SCT phase *b*

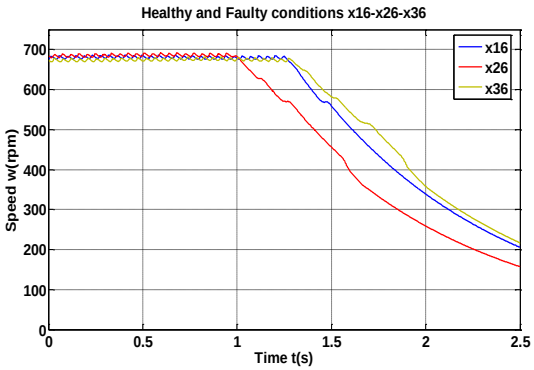


Fig. 12. Speed before and after phase-to-phase short circuit

### *B. Fault Severity Index (FSI)*

Signal processing plays a crucial role in computing an index directly related to the fault severity or to stating its occurrence. Incipient turn-to-turn fault of stator winding has been considered the most challenging fault [2], [4], [9] and [21]. Furthermore, turn faults are very difficult to detect at their initial stage. In order to carry out both an online or offline fault diagnosis scheme, it is highly desirable to use an easy-to-calculate fault severity index with a low computational burden. An index fault based on speed ripples in healthy and faulty conditions allows quantifying the severity of a turn-to-turn fault of stator winding; and it warns the user to implant proper method control (Fig. 13).

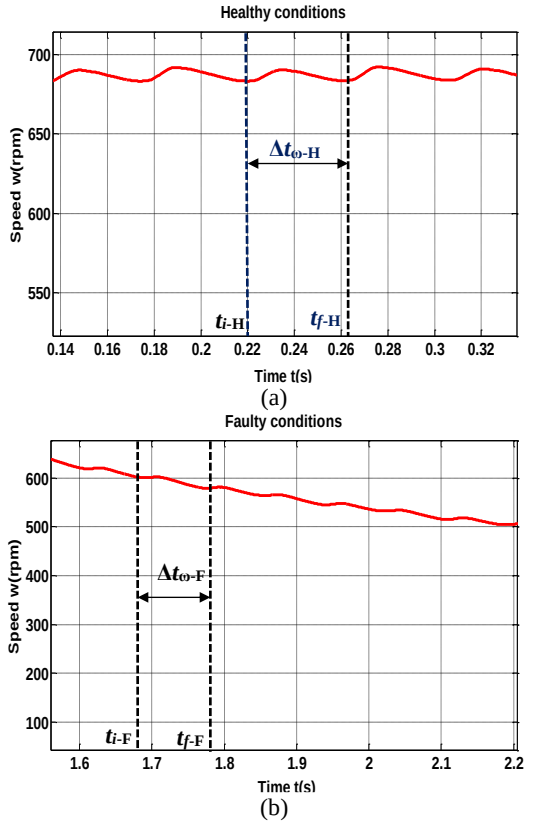


Fig. 13. Rotor Speed: a) healthy conditions, b) faulty conditions

The fault severity index (FSI) can now be defined as:

$$FSI = 1 - \frac{\Delta t_{\omega - H}}{\Delta t_{\omega - F}} \tag{13}$$

with

$$\begin{cases} \Delta t_{\omega-H} = t_{f-H} - t_{i-H} \\ \Delta t_{\omega-F} = t_{f-F} - t_{i-F} \end{cases} \quad (14)$$

where $\Delta t_{\omega-H}$ and $\Delta t_{\omega-F}$ are the time of alternating speed signal in healthy and faulty conditions, respectively. $t_{i\text{-}H}$ and $t_{f\text{-}H}$, are the initial and final times in healthy conditions; and $t_{i\text{-}F}$ and $t_{f\text{-}F}$, are the initial and final times in faulty conditions.

Table 4 shows the fault severity index in different experimental tests for two faulty phases. For example, in the case of x14 fault (5% of short circuited turns of phase *a* with 7% of short circuited turns of phase *b*) we observe an increase of $\Delta t_{\omega}$ from 0.045s to 0.06s which gives a considerable value of fault severity index (FSI=0.2467). If the number of short circuited turns of the two faulty phases increases (case of x15 and x16), the faulty severity index increases significantly as it can be seen in rows two and three of Table4. Even in case of x24, x25 and x26, the value of FSI significantly increases as the number of short-circuited turns is increased. Finally, in the last set of tests (x34, x35 and x36), the FSI increases significantly and the fault becomes more severe than in the previous experiments.

TABLE 4
EXTRACTED PARAMETERS USED TO CALCULATE FAULT SEVERITY INDEX

| **type** | $t_{i\_H}$, s | $t_{f\_H}$, s | $t_{i\_F}$, s | $t_{f\_F}$, s | $\Delta t_{\omega\_H}$, s | $\Delta t_{\omega\_F}$, s | ***FSI*** |
|---|---|---|---|---|---|---|---|
| x14 | 0.0876 | 0.1328 | 1.696 | 1.756 | 0.0452 | 0.0600 | 0.2467 |
| x15 | 0.0961 | 0.1425 | 1.812 | 1.887 | 0.0464 | 0.0750 | 0.3813 |
| x16 | 0.0880 | 0.1317 | 1.301 | 1.467 | 0.0437 | 0.1660 | 0.7367 |
| x24 | 0.0586 | 0.1043 | 1.529 | 1.613 | 0.0457 | 0.0840 | 0.4560 |
| x25 | 0.0762 | 0.1190 | 1.658 | 1.750 | 0.0428 | 0.0920 | 0.5348 |
| x26 | 0.0592 | 0.1042 | 1.115 | 1.254 | 0.0450 | 0.1390 | 0.6763 |
| x34 | 0.0669 | 0.1120 | 1.715 | 1.850 | 0.0451 | 0.1350 | 0.6659 |
| x35 | 0.0725 | 0.1189 | 1.400 | 1.596 | 0.0464 | 0.1960 | 0.7633 |
| x36 | 0.0646 | 0.1057 | 1.658 | 1.905 | 0.4110 | 0.2470 | 0.8336 |

## VI. CONCLUSION

This paper analyzed the consequences of the short circuit faults between two phases in permanent magnet synchronous motors; and it presented a simple method based on speed ripples to detect incipient turn-to-turn short circuit faults in two stator phases. As can be concluded by the analysis of the experimental results, the increase in the number of shorted turns in two faulty phases produces an increase in both the speed ripples frequency and the fault severity index. Thus, it is important to mention that in the fault detection method presented above, there is no need to know the details of the machine parameters. Also, this technique is able to rapidly detect incipient faults from about 5% of the winding in short circuits. It appears to be well adapted for PM synchronous motors health monitoring and interturn fault diagnosis.

## REFERENCES

[1] Y. Da, X. Shi and M. Krishnamurthy, "A new approach to fault diagnosis for permanent magnet synchronous machines using electromagnetic signature analysis," *IEEE Transactions on Power Electronics*, vol. 28, no. 8, pp.4104-4112, 2013.

[2] J. Hong, S. Park, D. Hyun, T. Kang, S. Lee, C. Kral and A. Haumer, "Detection and classification of rotor demagnetization and eccentricity faults for PM synchronous motors," *IEEE Transactions on Industry Applications*, vol. 48, no. 3, pp.923-932, 2012.

[3] K. Kim, D. Choi, B. Gu and I. Jung, "Fault model and performance evaluation of an inverter-fed permanent magnet synchronous motor under winding shorted turn and inverter switch open," *IET Electronic Power Applications*, vol. 4, no. 4, pp.214-225, 2010.

[4] A. Sarikhani and O. Mohammed, "Inter-turn fault detection in PM synchronous machines by physics-based back electromotive force estimation,"*IEEE Transactions on Industrial Electronics*, vol. 60, no. 8, pp.3472-3484, 2013.

[5] H. Saavedra, J. Urresty, J. Riba and L. Romeral, "Detection of interturn faults in PMSMs with different winding configurations," *Energy Conversion and Management*, vol. 79, pp.534-542, 2014.

[6] B. Gu, J. Choi and I. Jung, "Development and analysis of interturn short fault model of PMSMs with series and parallel winding connections," *IEEE Transactions on Power Electronics*, vol. 29, no. 4, pp.2016-2026, 2014.

[7] J. Urresty, J. Riba and L. Romeral, "Diagnosis of interturn faults in PMSMs operating under nonstationary conditions by applying order tracking filtering," *IEEE Transactions on Power Electronics*, vol. 28, no. 1, pp.507-515, 2013.

[8] I. Jeong, B. Hyon and K. Nam, "Dynamic modeling and control for SPMSMs with internal turn short fault," *IEEE Transactions on Power Electronics*, vol. 28, no. 7, pp.3495-3508, 2013.

[9] C. Wang, X. Liu and Z. Chen, "Incipient stator insulation fault detection of permanent magnet synchronous wind generators based on Hilbert-Huang transformation," *IEEE Transactions on Magnetics*, vol. 50, no. 11, pp. 1-4, 2014.

[10] F. Meiguet, E. Semail, X. Kestelyn, Y. Mollet and J. Gyselinck, "Change-detection algorithm for short-circuit fault detection in closed-loop AC drives," *IET Electric Power Applications*, vol. 8, no. 8, pp.165-177, 2014.

[11] M. Eftekhari, M. Moallem, S. Sadri and M. Hsieh, "Online detection of induction motor's stator winding short-circuit faults," *IEEE Systems Journal*, vol. 8, no. 4, pp.1272-1282, 2014.

[12] W. Liu, L. Liu, I. Chung, D. Cartes and W. Zhang, "Modeling and detecting the stator winding fault of permanent magnet synchronous motors," *Simulation Modelling Practice and Theory*, vol. 27, pp.1-16, 2012.

[13] M. Mazzoletti, G. Bossio, C. De Angelo and D. Espinoza-Trejo, "A model-based strategy for interturn short-circuit fault diagnosis in PMSM," *IEEE Transactions on Industrial Electronics*, vol. 64, no. 9, pp.7218-7228, 2017.

[14] B. Du, S. Wu, S. Han and S. Cui, "Interturn fault diagnosis strategy for interior permanent-magnet synchronous motor of electric vehicles based on digital signal processor," *IEEE Transactions on Industrial Electronics*, vol. 63, no. 3, pp.1694-1706, 2016.

[15] J. Urresty, J. Riba, L. Romeral and J. Ortega, "Mixed resistive unbalance and winding interturn faults model of permanent magnet synchronous motors," *Electrical Engineering*, vol. 97, pp.75-85, 2015.

[16] S. Saleh, R. Ahshan and M. Rahman, "Performance evaluation of an embedded d-q WPT-based digital protection for IPMSM drives," *IEEE Transactions on Industry Applications*, vol. 50, no. 3, pp.2277-2291, 2014.

[17] A. Gandhi, T. Corrigan and L. Parsa, "Recent advances in modeling and online detection of stator interturn faults in electrical motors," *IEEE Transactions on Industrial Electronics*, vol. 58, no. 5, pp.1564-1575, 2011.

[18] J. Antonio-Daviu, P. Rodriguez, M. Guasp, M. Sanchez and A. Arkkio, "Detection of combined faults in induction machines with stator parallel branches through the DWT of the startup current," *Mechanical Systems and Signal Processing*, vol. 23, pp.2336-2351, 2009.

[19] G. Li, S. Hloui, J. Ojeda, E. Hoang, M. Lecrivain, M. Gabsi and Z. Zhu, "Excitation winding short-circuits in hybrid excitation permanent magnet motor," *IEEE Transactions on Energy Conversion*, vol. 29, no. 3, pp.567-575, 2014.

[20] B. Aubert, J. Régnier, S. Coux and D. Alejo, "Kalman-filter-based indicator for online interturn short circuits detection in permanent magnet synchronous generators," *IEEE Transactions on Industrial Electronics*, vol. 26, no. 3, pp.1921-1930, 2015.

[21] P. Arumugan, T. Hamiti and C. Gerada, "Modeling of different winding configurations for fault-tolerant permanent magnet machines to restrain interturn short circuit current," *IEEE Transactions on Energy Conversion*, vol. 27, no. 2, pp.351-361, 2012.

[22] D. Progovac, L. Wang and G. Yin, "Parameter estimation and reliable fault detection of electric motors," *Control Theory and Technology*, vol. 12, no. 2, pp.110-121, 2014.

[23] Y. Cho, K. Lee, J. Song and Y. Lee, "Torque ripple minimization and fast dynamic scheme for torque predictive control of permanent magnet synchronous motors," *IEEE Transactions on Power Electronics*, vol. 30, no. 4, pp.2182-2190, 2015.

[24] W. Chi, M. Cheng, "Implementation of a sliding-mode-based position sensorless drive for high-speed micro permanent-magnet synchronous motors," *ISA Transactions*, vol. 53, pp.444-453, 2014.

[25] M. Ggaballah, "Design and implementation of space vector PWM inverter based on a low cost microcontroller," *Arabian Journal for Science and Engineering*, vol. 38, pp.3059-3070, 2013.

[26] A. Khlief, M. Boussak and A. Chaari, "A MRAS-based stator resistance and speed estimation for sensorless vector controlled IPMSM drive," *Electric Power Systems Research*, vol. 108, pp.1-15, 2014.

[27] K. Chen, J. Hu, C. Tang and T. Shen, "A novel switching strategy for FOC motor drive using multi-dimensional feedback quantization," *Control Engineering Practice*, vol. 20,pp.196-204, 2012.